Ultimate capacity of I-sections under combined loading – Part 2: Parametric studies and CSM design

Xiang Yun [a], Leroy Gardner [b], Nicolas Boissonnade [c]

[a] Department of Civil and Environmental Engineering, Imperial College London, SW7 2AZ, UK.

Email: x.yun14@imperial.ac.uk

[b] Department of Civil and Environmental Engineering, Imperial College London, SW7 2AZ, UK.

Email: leroy.gardner@imperial.ac.uk (Corresponding author)

[c] Department of Civil and Water Engineering, Laval University, Quebec, Canada

Email: nicolas.boissonnade@gci.ulaval.ca

Abstract

The second part of the study on the ultimate capacity of hot-rolled steel I-sections under combined compression and bending moment, focussing on parametric studies and design, is presented herein. An extensive numerical parametric study was carried out, using the verified finite element (FE) models from the companion paper, to generate further structural performance data for specimens with different steel grades, cross-section slendernesses and loading cases. The numerical results together with the experimental results were then used to assess the accuracy of two codified design methods: the European Standard EN 1993-1-1 (2005) and the American Specification AISC-360-16 (2016). The design strengths predicted by the current design standards were found to be generally rather conservative and scattered when

applied to non-slender cross-sections, owing principally to the neglect of material strain hardening and reserve capacities between the classification limits. To improve the accuracy and efficiency of the design rules, the continuous strength method (CSM) – a deformation-based design approach which relates the resistance of a cross-section to its deformation capacity – was extended to cover the design of hot-rolled steel I-sections under combined loading, underpinned by both the experimentally and numerically derived ultimate capacities. Overall, the CSM was shown to offer more accurate and consistent predictions than the current design provisions. Finally, reliability analysis was performed to evaluate the reliability level of the design rules.

1. Introduction

In the design of hot-rolled structural steelwork, cross-section classification is a fundamental feature in most current codes of practice, such as the European Standard EN 1993-1-1 (EC3) [1] and the American Specification AISC-360-16 [2], and determines the extent to which the strength and deformation capacity of a cross-section are limited by the effects of local buckling. Traditionally, classification or slenderness limits have been expressed in terms of width-to-thickness ratios for individual plates of a cross-section, considering boundary conditions – internal (stiffened) or outstand (unstiffened) elements and stress patterns. There has been considerable research on the behaviour and strength of I-sections under combined loading over the past decades, with the aim of assessing and improving the current design rules. Revised slenderness limits for I cross-sections have been proposed by [3,4], accounting for the effects of web-flange interaction. Dawe and Kulak [5] investigated the local buckling behaviour of

beam-columns and proposed web slenderness limits that consider the interaction effects of constituent plate elements and the applied load level. Kettler [6] performed a series of tests to investigate the cross-section resistance of semi-compact (Class 3) I-sections and rectangular hollow sections, and developed a design proposal to describe the transition from plastic to elastic cross-section resistance. Interaction curves for slender I-sections subjected to combined axial load and bending moment were systematically studied by Salem et al. [7] and Hasham and Rasmussen [8,9], where conservatism in existing codified design provisions was highlighted and improved interaction curves were proposed, resulting in more accurate resistance predictions.

The current codified stepwise approach to the classification of structural steel cross-sections ignores the interaction between the elements, such as the flanges and web, and fails to account for the inherent continuous relationship between the cross-section resistance and its slenderness; additionally, there is limited or no knowledge of the deformations (or strains) required to reach a given capacity, such as the plastic moment capacity in bending, which will vary with cross-section shape, axis of bending, type of steel, and so on. In recent years, a new deformation-based design approach termed the continuous strength method (CSM) has been proposed [10-12] to address these shortcomings. The CSM replaces the concept of cross-section classification with a continuous non-dimensional measure of the cross-section deformation capacity and adopts a simple elastic, linear hardening material model which allows for the beneficial influence of strain hardening. Owing to the existence of a yield plateau, the CSM bi-linear material model is less suitable for hot-rolled carbon steels. Thus a more appropriate quad-linear material model [13] has been developed for hot-rolled carbon steels, which exhibits a yield point, followed by a yield plateau and a strain hardening region; this model has been incorporated into the CSM design framework for hot-rolled steel cross-sections under the

isolated loading conditions of compression and bending [14,15]. In this paper, the application

of the CSM to the case of hot-rolled steel I-sections under combined loading is explored. The

accuracy of different design methods, including EC3 [1], AISC [2] and the proposed CSM, are

then assessed based on the test results presented in the companion paper [16] and numerical

parametric data derived herein, using the validated finite element (FE) models.

2. Parametric studies

In this section, an extensive numerical parametric study is presented based on the FE models

validated in the companion paper [16] to expand the available results over a wider range of I-

section geometries, cross-section slendernesses and loading combinations. A detailed

description of the FE models and their validation against experimental results, including the

ultimate loads, load-deformation curves and failure modes, were reported in the companion

paper [16], while the principal aspects relating to the parametric studies are presented herein.

The measured stress-strain curves from the flange tensile coupons for the different material

grades (S235 and S355), as reported in the companion paper [16], were adopted in the

parametric studies. The length of all FE models was set equal to three times the average cross-

section dimensions. For each steel grade, the height (H) and the corner radii (r_i) of the

specimens were kept constant at 200 mm and 15 mm, respectively, while four cross-section

aspect ratios H/B of 1.0, 1.5, 2.0 and 2.5 were considered by varying the width of the flanges

(B) from 200 mm to 80 mm. Maintaining the cross-section outer dimensions, the effect of local

cross-section slenderness was investigated by varying the flange and web thicknesses (t_f and

t_w), resulting in a range of cross-section slenderness values $\bar{\lambda}_p$ between 0.17 and 0.68. The

cross-section slenderness $\bar{\lambda}_p$ is defined as $\bar{\lambda}_p = \sqrt{f_y / \sigma_{cr}}$, where σ_{cr} is the elastic buckling stress

of the cross-section under the applied loading conditions, which may be obtained numerically

(e.g. using the finite strip software CUFSM, as adopted in the present study) or using approximate expressions [17]. Note that $\bar{\lambda}_\text{p} = 0.68$ is the boundary between slender and non-slender cross-sections in the CSM [10], and the present study focuses primarily on non-slender sections where local buckling occurs after yielding. For each cross-section, a combination of 10 different initial loading eccentricities, which varied from 10 to 50 mm in 10 mm intervals and 100 to 500 mm in 100 mm intervals for the loading scenarios of 0, 30, 45 and 60 degrees and from 10 to 100 mm in 10 mm intervals for the loading scenario of 90 degrees, was considered in the parametric studies, leading to a wide range of loading conditions (i.e. ratios of axial force to bending moment). The 0 and 90 degree cases represent the I-sections under major axis bending plus compression and minor axis bending plus compression, respectively, while the remaining loading scenarios consider I-sections under biaxial bending plus compression. Local geometric imperfections were included in the models and were assumed to be of the form of the lowest elastic buckling mode shape in compression with an odd number buckling half-waves, with an imperfection amplitude of $c/200$, where c is the flat width of the most slender constituent plater element in the cross-section under compression (i.e. that with the highest value of $\sqrt{f_\text{y}/\sigma_\text{cr}}$ under compression). In terms of residual stresses, the ECCS model, as described in the companion paper [16], was incorporated into the FE models. A total of 1500 numerical results were generated, with 750 for each steel grade, including 300 for I-sections under uniaxial bending plus compression and 450 for biaxial bending plus compression. The numerical results, combined with the collected experimental data [16], are analysed in the following sections and used to assess and develop design expressions for hot-rolled steel I-sections under combined loading.

3. Assessment of current design methods and extension of the CSM

In this section, ultimate capacities from the experiments and FE simulations on hot-rolled steel I-sections under combined loading have been used to examine the accuracy of the codified design provisions of EC3 [1] and AISC [2]. Then, extension of the CSM to the case of hot-rolled steel I-sections subjected to the combined actions of compression and bending moment is undertaken. Key numerical comparisons, including the mean and the coefficient of variation (COV), of the axial load ratio, $N_{u,test/FE}/N_{u,pred}$, for each design method are reported in Table 1, where $N_{u,test/FE}$ is the test (or FE) axial load corresponding to the distance from the origin to the test (or FE) data point, and $N_{u,pred}$ is the predicted axial load corresponding to the projection from the origin to the associated intersection with the design interaction curve, as graphically defined in Fig. 1. As shown in Fig. 1, a value of the axial load ratio $N_{u,test/FE}/N_{u,pred}$ greater than unity indicates that the design interaction curve falls short of the corresponding test (or FE) data point and thus results in a safe-sided strength prediction, and vice versa. Note that the comparisons were performed using the measured geometric and material properties of the tested and modelled cross-sections, with all partial safety factors set to unity.

3.1. European Code EN 1993-1-1 (EC3)

For hot-rolled steel I-sections subjected to combined compression and bending moment, EN 1993-1-1 [1] employs a linear elastic interaction expression for Class 3 cross-sections, assuming that failure occurs when the maximum stress in the cross-section reaches the yield stress f_y, as given by Eq. (1), in which N_{Ed} is the applied design axial load, M_{Ed} is the applied design bending moment, including the second order bending moment due to the lateral mid-height deflection, N_y is the yield load equal to the product of the gross cross-sectional area A and the yield stress f_y, M_{el} is the elastic moment capacity, and the subscripts 'y' and 'z' refer to the major and minor axis, respectively, and the subscript 'Rd' denotes design resistance.

$$\frac{N_{\text{Ed}}}{N_{\text{y,Rd}}} + \frac{M_{\text{Ed,y}}}{M_{\text{el,y,Rd}}} + \frac{M_{\text{Ed,z}}}{M_{\text{el,z,Rd}}} \leq 1 \tag{1}$$

For Class 1 and 2 cross-sections, the beneficial effect of plastic stress redistribution is allowed for by employing a nonlinear interaction expression, as given by Eq. (2), where the interaction power parameters are taken as $\alpha = 2$ and $\beta = 5n \geq 1$, in which n is the ratio of design axial load to yield load N_{Ed}/N_y, and $M_{\text{N,y}}$ and $M_{\text{N,z}}$ are the reduced plastic moment resistances about the major and minor axis due to the presence of axial load, as given by Eqs. (3) and (4), respectively. In Eqs. (3) and (4), M_{pl} represents the plastic bending capacity assuming full plasticity throughout the cross-section at failure and a is the ratio of the web area to the gross cross-section area (with a maximum value of 0.5), which takes account of the influence of the geometry of the I-section.

$$\left(\frac{M_{\text{Ed,y}}}{M_{\text{N,y,Rd}}}\right)^{\alpha} + \left(\frac{M_{\text{Ed,z}}}{M_{\text{N,z,Rd}}}\right)^{\beta} \leq 1 \tag{2}$$

$$M_{\text{N,y,Rd}} = M_{\text{pl,y,Rd}} \frac{1-n}{1-0.5a} \leq M_{\text{pl,y,Rd}} \tag{3}$$

$$M_{\text{N,z,Rd}} = \begin{cases} M_{\text{pl,z,Rd}} & \text{for } n \leq a \\ M_{\text{pl,z,Rd}} \left[1 - \left(\frac{n-a}{1-a}\right)^2\right] & \text{for } n > a \end{cases} \tag{4}$$

The uniaxial bending plus compression test and FE results are normalised by their respective yield loads N_y and plastic moment capacities M_{pl} and are plotted together with the codified EC3 interaction curves in Figs 2 and 3 for major axis and minor axis bending, respectively. Since the interaction expressions (Eqs. (3) and (4)) for Class 1 and 2 cross-sections depend on the

geometric properties of the cross-sections through the ratio of web area to gross cross-sectional area a, and the ratio of M_{el}/M_{pl}, which varied among the considered sections, the average interaction curves are depicted for illustration purposes. For Class 1 and 2 sections, the EC3 design strengths are shown to be generally conservative, particularly for the stockier cross-sections, due largely to the conservative strength predictions of the end points of the design interaction curves, i.e. the compression and bending resistances, which are determined without considering the beneficial effects of strain hardening. For Class 3 sections, EC3 utilizes a linear interaction expression and limits the bending resistances to elastic moment capacities M_{el}; ignores the partial spread of plasticity and thus again yields conservative strength predictions, as shown in Figs 2 and 3. For the grade S235 steel, which exhibits a higher degree of strain hardening and a shorter length of yield plateau compared with grade S355 steel, a more pronounced level of conservatism is present in the EC3 predictions for the stockier cross-sections, as shown in Figs 2 and 3. However, for the less stocky cross-sections, where strain hardening is not experienced, the differences due to the influence of yield stresses are seen to be negligible. As reported in Table 1, the mean ratios of $N_{u,test/FE}/N_{u,EC3}$ are equal to 1.07, 1.45 and 1.46, with the coefficient of variation (COV) of 0.11, 0.31 and 0.32, for hot-rolled steel I-sections under major axis bending moment plus compression, minor axis bending plus compression and biaxial bending plus compression, respectively. The scatter and conservatism of the EC3 predictions are related to the omission of strain hardening, the inaccuracy of the slenderness limits and the shape of the interaction curves.

3.2. American Specification AISC 360-16

Unlike EC3, which takes account of the stress patterns in the individual compressed plates for the classification of cross-sections under combined loading, the AISC Specification [2] only directly considers the fundamental scenarios of pure compression and pure bending. The

interaction of bending and compression in hot-rolled steel I-sections is covered by Eqs. (5) and (6) in AISC 360-16, where, in the absence of member buckling (i.e. for cross-section resistance, which is the focus of the present study), N_c and M_c are the nominal cross-sectional axial compression and bending resistances, respectively. The design rules in AISC 360-16 for determining compression strengths of non-slender cross-sections are generally the same as those in EC3, except that the AISC replaces the yield stress with flexural buckling stress to account for the second order effects, though the difference is negligible for short columns, as studied herein. For the calculation of bending resistances, both EC3 and the AISC Specification adopt the plastic moment capacity M_{pl} for stocky (compact) cross-sections, i.e. Class 1 and 2 cross-sections in EC3. However, for non-compact sections (equivalent to Class 3 sections in EC3), the bending resistances are limited to M_{el} in EC3, while the AISC Specification accounts for the partial spread of plasticity in determining the bending capacities M_c. Note that a revision to EC3 to include a similar provision for Class 3 cross-sections is anticipated [18].

$$\frac{N_{Ed}}{N_c} + \frac{8}{9}\left(\frac{M_{Ed,y}}{M_{c,y}} + \frac{M_{Ed,z}}{M_{c,z}}\right) \leq 1, \text{for } \frac{N_{Ed}}{N_c} \geq 0.2 \tag{5}$$

$$\frac{N_{Ed}}{2N_c} + \frac{M_{Ed,y}}{M_{c,y}} + \frac{M_{Ed,z}}{M_{c,z}} \leq 1, \text{for } \frac{N_{Ed}}{N_c} < 0.2 \tag{6}$$

For Class 1 and 2 sections, the end points of the interaction curves, i.e. the cross-section resistances under pure compression and bending, are similar in the AISC Specification and EC3, but the bilinear interaction curve employed in AISC is more conservative than those used in EC3, which contain a plateau in the region of low axial force and are more convex in the region of intermediate and high axial force. As a result, the AISC Specification yields more conservative strength predictions than EC3 for Class 1 and 2 sections. Owing to the different

slenderness limits and approaches to classify cross-sections in AISC 360-16 and EC3, all the

Class 3 cross-sections (according to EC3) investigated in the present study are classified as

compact (i.e. Class 1 or 2) cross-sections according to AISC. This in return leads to improved

design resistances from the AISC predictions compared to the EC3 predictions, which are

shown to be unduly conservative for Class 3 cross-sections, as illustrated in Figs 2 and 3. The

accuracy of the AISC Specification is assessed in Table 1 and Figs 4 and 5, where the

experimental and numerical results are normalised by their AISC design resistances (N_c and

M_c) and compared against the AISC interaction curve for major and minor axis bending plus

compression, respectively. As can be seen from Table 1, the mean test (FE) to predicted

resistance ratios $N_{u,test/FE}/N_{u,AISC}$ are 1.09 and 1.31, with corresponding COV values of 0.09 and

0.11 for major and minor axis bending plus compression, respectively. Compared to the

uniaxial bending cases, conservatism increases in the case of resistance predictions against

biaxial bending plus compression, with a mean test (FE)-to-predicted resistance ratio of 1.41

and a corresponding COV of 0.09. Overall, the AISC Specification offers improved mean

resistance predictions and reduced scatter compared to the EN 1993-1-1 design rules, though

still shows significant conservatism.

3.3. Continuous Strength Method (CSM)

The CSM [10-12] is a deformation-based design approach that can utilize the beneficial effects

of strain hardening in the calculation of cross-section resistances. To date, the method has been

established and verified for the design of stainless steel and aluminium alloy cross-sections,

and is included in North American and European design provisions [19,20]. Extension of the

method to hot-rolled steel cross-sections under the isolated loading conditions of compression

and bending has been set out in [14], employing a material model [13] suitable for capturing

the stress-strain characteristics of hot-rolled steels. A detailed description of the derivation of

the CSM resistance equations for hot-rolled steel cross-sections in compression and bending can be found in [14], while a brief summary of the provisions is given in the following paragraphs.

There are two key components of the CSM: (1) a continuous design base curve defining the maximum strain ε_{csm} that a cross-section can sustain as a function of the cross-section slenderness $\bar{\lambda}_p$ and (2) a material model that considers strain hardening. The cross-section deformation capacity, which is defined in a normalised form as ε_{csm} divided by the yield strain ε_y, can be determined from the base curve, as given by Eq. (7) for non-slender plated sections. Two upper bounds are placed on the normalised cross-section deformation capacity, $\varepsilon_{csm}/\varepsilon_y \leq 15$ and $\varepsilon_{csm}/\varepsilon_y \leq C_1\varepsilon_u/\varepsilon_y$, where ε_u is the strain at the ultimate tensile stress and C_1 is a coefficient corresponding to the adopted CSM material model [13]; the first limit of 15 corresponds to the material ductility requirement in EN 1993-1-1 [1], but is essentially restricting the strains to tolerable levels within a design (and alternative values could be employed), while the second limit of $C_1\varepsilon_u/\varepsilon_y$ avoids over-predictions of material strength from the stress-strain model. The cross-section slenderness $\bar{\lambda}_p$ within the CSM is defined in non-dimensional form as the square root of the yield stress f_y divided by the elastic buckling stress σ_{cr} (see Eq. (8)). The elastic buckling stress of the cross-section should be determined considering the effects of plate element interaction [17,21], as discussed earlier, but could conservatively be taken as the local buckling stress of the most slender individual plate element in the cross-section under the applied loading conditions, as set out in [22].

$$\frac{\varepsilon_{csm}}{\varepsilon_y} = \frac{0.25}{\bar{\lambda}_p^{3.6}}, \text{ but } \frac{\varepsilon_{csm}}{\varepsilon_y} \leq \min\left(15, \frac{C_1\varepsilon_u}{\varepsilon_y}\right) \quad \text{for } \bar{\lambda}_p \leq 0.68 \tag{7}$$

$$\bar{\lambda}_{\mathrm{p}} = \sqrt{f_{\mathrm{y}} / \sigma_{\mathrm{cr}}} \tag{8}$$

The first three stages of the adopted quad-linear material model [13], which was based upon and calibrated against data from over 500 experimental stress-strain curves collected from the global literature [13], as depicted in Fig. 6 and described by Eq. (9), is employed as the CSM material model that takes account of both the yield plateau and the strain hardening of hot-rolled steels. In Fig. 6, E is the Young's modulus, f_{y} is the yield stress, $\varepsilon_{\mathrm{y}} = f_{\mathrm{y}}/E$ is the yield strain, f_{u} and ε_{u} are the ultimate tensile stress and the corresponding ultimate strain, respectively, $\varepsilon_{\mathrm{sh}}$ is the strain hardening strain where the yield plateau ends and subsequently the strain hardening initiates, C_1 is a material coefficient that defines a cut-off strain in the CSM base curve (see Eq. (7)) to avoid over-predicting the failure strength from the quad-linear model, and the material coefficient C_2 is utilised to determine the strain hardening modulus E_{sh}, as given in Eq. (10).

$$f(\varepsilon) = \begin{cases} E\varepsilon & \text{for } \varepsilon \leq \varepsilon_{\mathrm{y}} \\ f_{\mathrm{y}} & \text{for } \varepsilon_{\mathrm{y}} < \varepsilon \leq \varepsilon_{\mathrm{sh}} \\ f_{\mathrm{y}} + E_{\mathrm{sh}}(\varepsilon - \varepsilon_{\mathrm{sh}}) & \text{for } \varepsilon_{\mathrm{sh}} < \varepsilon \leq C_1\varepsilon_{\mathrm{u}} \\ f_{C_1\varepsilon_{\mathrm{u}}} + \dfrac{f_{\mathrm{u}} - f_{C_1\varepsilon_{\mathrm{u}}}}{\varepsilon_{\mathrm{u}} - C_1\varepsilon_{\mathrm{u}}}(\varepsilon - C_1\varepsilon_{\mathrm{u}}) & \text{for } C_1\varepsilon_{\mathrm{u}} < \varepsilon \leq \varepsilon_{\mathrm{u}} \end{cases} \tag{9}$$

$$E_{\mathrm{sh}} = \frac{f_{\mathrm{u}} - f_{\mathrm{y}}}{C_2\varepsilon_{\mathrm{u}} - \varepsilon_{\mathrm{sh}}} \tag{10}$$

The quad-linear model utilises three basic material parameters, E, f_{y} and f_{u}, which are readily available to engineers in material standards, as well as additional material parameters (ε_{u}, $\varepsilon_{\mathrm{sh}}$, C_1 and C_2), for which predictive expressions are given by Eqs. (11)-(14), respectively.

$$\varepsilon_{\mathrm{u}} = 0.6\left(1 - \frac{f_{\mathrm{y}}}{f_{\mathrm{u}}}\right) \text{ , but } \varepsilon_{\mathrm{u}} \geq 0.06 \text{ for hot-rolled steels} \tag{11}$$

$$\varepsilon_{\mathrm{sh}} = 0.1\frac{f_{\mathrm{y}}}{f_{\mathrm{u}}} - 0.055 \text{ , but } 0.015 \leq \varepsilon_{\mathrm{sh}} \leq 0.03 \tag{12}$$

$$C_1 = \frac{\varepsilon_{\mathrm{sh}} + 0.25(\varepsilon_{\mathrm{u}} - \varepsilon_{\mathrm{sh}})}{\varepsilon_{\mathrm{u}}} \tag{13}$$

$$C_2 = \frac{\varepsilon_{\mathrm{sh}} + 0.4(\varepsilon_{\mathrm{u}} - \varepsilon_{\mathrm{sh}})}{\varepsilon_{\mathrm{u}}} \tag{14}$$

Within the CSM design framework, cross-section resistances are determined utilising the strain ratio $\varepsilon_{\mathrm{csm}}/\varepsilon_{\mathrm{y}}$ from the design base curve (Eq. (7)), together with the adopted CSM material model (Eq. (9)). The CSM limiting stress f_{csm} corresponding to the CSM strain can be determined using Eq. (15) and f_{csm} is then utilised to derive the CSM cross-section capacities. The CSM compression resistance $N_{\mathrm{csm,Rd}}$ is equal to the product of the CSM limiting stress f_{csm} and the gross cross-section area A, divided by the partial factor for cross-section resistance γ_{M0} with a recommended value of unity for hot-rolled steel [1], as given by Eq. (16).

$$f_{\mathrm{csm}} = \begin{cases} f_{\mathrm{y}} & \text{for } \varepsilon_{\mathrm{y}} < \varepsilon_{\mathrm{csm}} \leq \varepsilon_{\mathrm{sh}} \\ f_{\mathrm{y}} + E_{\mathrm{sh}}(\varepsilon_{\mathrm{csm}} - \varepsilon_{\mathrm{sh}}) & \text{for } \varepsilon_{\mathrm{sh}} < \varepsilon_{\mathrm{csm}} \leq C_1\varepsilon_{\mathrm{u}} \end{cases} \tag{15}$$

$$N_{\mathrm{csm,Rd}} = \frac{Af_{\mathrm{csm}}}{\gamma_{\mathrm{M0}}} \tag{16}$$

The CSM bending resistance of a cross-section $M_{csm,Rd}$ depends upon whether or not the CSM strain ε_{csm} enters into the strain hardening regime (i.e. whether or not $\varepsilon_{csm} > \varepsilon_{sh}$). If $\varepsilon_{csm} \leq \varepsilon_{sh}$, strain hardening is not experienced and the expressions for the determination of $M_{csm,Rd}$ are given by Eqs. (17) and (18) for major and minor axis bending, respectively, where W_{el} and W_{pl} are the elastic and plastic section modulus, respectively, and α is a dimensionless coefficient, related to the cross-section shape and the axis of bending, with the recommended values of 2 and 1.2 for I-sections in major and minor axis bending, respectively.

$$M_{csm,y,Rd} = \frac{W_{pl,y} f_y}{\gamma_{M0}} \left[1 - \left(1 - \frac{W_{el,y}}{W_{pl,y}} \right) \middle/ \left(\frac{\varepsilon_{csm}}{\varepsilon_y} \right)^\alpha \right], \quad \text{for } \varepsilon_y < \varepsilon_{csm} \leq \varepsilon_{sh} \quad (17)$$

$$M_{csm,z,Rd} = \frac{W_{pl,z} f_y}{\gamma_{M0}} \left[1 - \left(1 - \frac{W_{el,z}}{W_{pl,z}} \right) \middle/ \left(\frac{\varepsilon_{csm}}{\varepsilon_y} \right)^\alpha \right], \quad \text{for } \varepsilon_y < \varepsilon_{csm} \leq \varepsilon_{sh} \quad (18)$$

For the stockier cross-sections where $\varepsilon_{csm} > \varepsilon_{sh}$, i.e. the outer fibre strain of the cross-section enters into the strain hardening region and the benefit from strain hardening can be exploited, the design formulae for $M_{csm,Rd}$ are given by Eqs. (19) and (20) for major and minor axis bending, respectively, where the values of the coefficient β are taken as 0.1 for major axis bending and 0.05 for minor axis bending.

$$M_{csm,y,Rd} = \frac{W_{pl,y} f_y}{\gamma_{M0}} \left[1 - \left(1 - \frac{W_{el,y}}{W_{pl,y}} \right) \middle/ \left(\frac{\varepsilon_{csm}}{\varepsilon_y} \right)^\alpha + \beta \left(\frac{\varepsilon_{csm} - \varepsilon_{sh}}{\varepsilon_y} \right)^2 \frac{E_{sh}}{E} \right], \quad \text{for } \varepsilon_{csm} > \varepsilon_{sh} \quad (19)$$

$$M_{csm,z,Rd} = \frac{W_{pl,z} f_y}{\gamma_{M0}} \left[1 - \left(1 - \frac{W_{el,z}}{W_{pl,z}} \right) \middle/ \left(\frac{\varepsilon_{csm}}{\varepsilon_y} \right)^\alpha + \beta \left(\frac{\varepsilon_{csm} - \varepsilon_{sh}}{\varepsilon_y} \right)^2 \frac{E_{sh}}{E} \right], \quad \text{for } \varepsilon_{csm} > \varepsilon_{sh} \quad (20)$$

The CSM resistance equations (Eqs. (17)-(20)) for the calculation of compression and bending in isolation have been carefully assessed in [14], revealing that the CSM provides more accurate and consistent predictions than the existing design provisions, especially for stockier cross-sections and for Class 3 sections in bending.

The accuracy in predicting the resistances of cross-sections under combined axial compression and bending moment depends largely on the accuracy to which the cross-section compression and bending resistances, which represent the end points of the interaction curves, can be determined. Recent studies into the cross-section resistance of stainless steel square and rectangular hollow sections under combined loading [23,24] showed that substantially improved predictions can be obtained by adopting the nonlinear N-M interaction expressions and coefficients in EC3 but replacing the plastic design resistances (N_y and M_{pl}) with the corresponding CSM predictions (N_{csm} and M_{csm}) as the end points for cross-sections with $\overline{\lambda}_p$ less than or equal to 0.6, and by adopting a linear design interaction formula for cross-sections with $\overline{\lambda}_p$ greater than 0.6. The possibility of applying a similar approach for hot-rolled steel I-sections is explored herein. The test and FE data points are normalised by the CSM end points in Figs 7 and 8. For cross-sections with $\overline{\lambda}_p \leq 0.6$, the proposed CSM interaction formulae are given by Eqs. (21) and (22) for hot-rolled steel I-sections under combined compression and uniaxial bending moment about the major and minor axis, respectively, and by Eqs. (23) for hot-rolled steel I-sections under biaxial bending plus compression, in which $M_{R,csm,y,Rd}$ and $M_{R,csm,z,Rd}$ are the reduced CSM bending resistances about major and minor axis in the presence of an axial load N_{Ed}. In these equations, n_{csm} is the ratio of the design axial force to the CSM cross-section compression resistance N_{Ed}/N_{csm}, α_{csm} and β_{csm} are the interaction coefficients whose values are taken from EC3 but based on the CSM end points with $\alpha_{csm} = 2$ and $\beta_{csm} = 5n_{csm} \geq 1$, and $a_{csm,w}$ and $a_{csm,f}$ are parameters that relate to the ratios of web area A_w and flange

area A_f to gross cross-section area A, respectively, and determine the plateau length of the interaction curves, i.e. $0.5a_{csm,w}$ for major axis bending plus compression and $a_{csm,f}$ for minor axis bending plus compression. A reduced upper limit of 0.25 is set on the parameters $a_{csm,w}$ and $a_{csm,f}$, as given by Eqs. (24) and (25) respectively, since the upper limit of 0.5 adopted in EC3 results in some unconservative predictions for cross-sections with large web area to gross cross-section area ratios (i.e. cross-sections with high aspect ratios).

$$M_{R,csm,y,Rd} = M_{csm,y,Rd} \frac{1-n_{csm}}{1-0.5a_{csm,w}}, \text{ but} \leq M_{csm,y,Rd} \tag{21}$$

$$M_{R,csm,z,Rd} = \begin{cases} M_{csm,z,Rd} & \text{for } n_{csm} \leq a_{csm,f} \\ M_{csm,z,Rd} \left[1 - \left(\frac{n_{csm} - a_{csm,f}}{1 - a_{csm,f}} \right)^2 \right] & \text{for } n_{csm} > a_{csm,f} \end{cases} \tag{22}$$

$$\left(\frac{M_{Ed,y}}{M_{R,csm,y}} \right)^{\alpha_{csm}} + \left(\frac{M_{Ed,z}}{M_{R,csm,z}} \right)^{\beta_{csm}} \leq 1, \quad \text{for } \overline{\lambda}_p \leq 0.6 \tag{23}$$

$$a_{csm,w} = \frac{A_w}{A}, \text{ but } a_{csm,w} \leq 0.25 \tag{24}$$

$$a_{csm,f} = \frac{A_f}{A} - 0.5, \text{ but } 0 \leq a_{csm,f} \leq 0.25 \tag{25}$$

For cross-sections with $\overline{\lambda}_p > 0.6$, strain hardening is less significant and the linear interaction curve, as given by Eq. (26), is proposed.

$$\frac{N_{\text{Ed}}}{N_{\text{csm,Rd}}} + \frac{M_{\text{Ed,y}}}{M_{\text{csm,y,Rd}}} + \frac{M_{\text{Ed,z}}}{M_{\text{csm,z,Rd}}} \leq 1, \quad \text{for } \overline{\lambda}_{\text{p}} > 0.6 \tag{26}$$

The ratios of test and FE resistances to predicted resistances according to the CSM and EC3 are plotted against cross-section slenderness $\overline{\lambda}_{\text{p}}$ in Figs 9-11 for hot-rolled steel I-sections under compression and major axis bending, minor axis bending and biaxial bending, respectively, while the corresponding comparisons between CSM and AISC predictions are shown in Figs 12-14. The comparisons reveal that the CSM offers more accurate capacity predictions than EC3 and AISC. The mean test (FE) to CSM predicted failure load ratios $N_{\text{u,test/FE}}/N_{\text{u,csm}}$, as reported in Table 1, are 1.05, 1.13 and 1.12 for hot-rolled steel I-sections under compression plus major axis bending, minor axis bending and biaxial bending, respectively, all of which are lower than the corresponding values resulting from the EC3 and AISC design calculations, thus indicating improved accuracy. The corresponding COV values of 0.08, 0.13 and 0.11 also show reduced scatter in comparison to EC3. Similar comparisons for the test results only are reported in Table 2, again highlighting the improved accuracy offered by the continuous strength method though the COV of its prediction for hot-rolled steel I-sections under minor axial bending plus compression is slightly higher than the corresponding value from EC3. Note the differences in mean and COV values between the comparisons of Tables 1 and 2 are due to the ranges of cross-section slenderness and combinations of loading considered – while the experiments only consider a limited number of isolated cases, the finite elements results cover the full range of both parameters.

In order to illustrate the influence of the applied combination of loading (i.e. the ratio of axial load to bending moment) on the strength predictions, the ratios of $N_{\text{u,test/FE}}/N_{\text{u,pred}}$ are plotted against an angle parameter θ in Figs 15-18 for hot-rolled steel I-sections under compression

and uniaxial bending moment. The angle parameter θ is introduced to describe the combination of axial load and bending moment and is defined by Eq. (27), where N_{Rd} and M_{Rd} are the cross-section compression and bending resistances, respectively, and $N_{\mathrm{u,pred}}$ and $M_{\mathrm{u,pred}}$ are the predicted axial load and bending moment corresponding to the projection from the origin to the associated intersection with the design interaction curve, as shown in Fig. 19. Based on the definition of θ, the pure bending case can be expressed as $\theta = 0°$ while the pure compression scenario can be represented by $\theta = 90°$, as indicated in Figs 15-18.

$$\theta = \tan^{-1}\left(\frac{N_{\mathrm{u,pred}}/N_{\mathrm{Rd}}}{M_{\mathrm{u,pred}}/M_{\mathrm{Rd}}}\right) \tag{27}$$

For I-sections in major axis bending plus compression, EC3 allows the plastic bending moment M_{pl} to be attained with axial load ratios n up to 0.25 (see Eq. (3) with the upper limit value of a being 0.5). However, this results in some unconservative resistance predictions for specimens with high ratios of web area to gross cross-section area and lower n ratios (i.e. $\theta \leq 20°$), as shown in Figs 2 and 15. This stems principally from the underestimation of the adverse effect of the axial load on the bending resistances of I-sections with high H/B ratios (i.e. cross-sections with large web area to gross cross-section area ratios a). With the adoption of an upper limit of 0.25 for a_{csm} in Eq. (21), the CSM yields more accurate strength predications than EC3 for the aforementioned specimens, as shown in Figs 7 and 15.

The comparisons in Fig. 16 generally reveal an increase in conservatism as the applied loading varies from pure compression to pure bending (i.e. as θ moves from 90° to 0°) for both the EC3 and CSM resistance predictions for I-sections in minor axis bending plus compression. The unduly conservative EC3 resistance predictions for Class 3 cross-sections (see the Class 3

points in Fig. 3 in relation to the linear interaction curve, which correspond to the points indicated in Figs 10 and 16) are caused by the sharp drop in predicted bending strength from M_{pl} to M_{el} in the conventional cross-section classification system. This concept has been replaced with the more rational cross-section deformation capacity in the CSM, which provide more accurate and consistent predictions, as shown in Figs 10 and 16. The CSM predictions do however remain rather conservative for combinations of loading with lower axial load ratios (i.e. $\theta \leq 10°$) – this is due primarily to the imposed strain ratio limit of $\varepsilon_{csm}/\varepsilon_y = 15$ for minor axis bending of I-sections [16]. This limit could, however, be adjusted depending on the level of plastic deformation that was deemed acceptable at the ultimate limit state in a given project. More strain hardening can be exploited for hot-rolled steel I-sections with lower ratios of axial load to minor axis bending if the strain ratio limit for minor axis bending is relaxed to 25 [16].

4. Reliability analysis

A reliability analysis was carried out in accordance with Annex D of EN 1990 [25] to assess the reliability level and required partial safety factor γ_{M0} for the existing design methods and the proposed CSM for hot-rolled steel I-sections under combined loading. The partial safety factor γ_{M0} has a recommended value of 1.0 for the design of hot-rolled steel cross-sections in EN 1993-1-1 [1]. A calculated (required) partial safety factor γ_{M0} below this value therefore indicates that the reliability requirements of EN 1990 [25] are met. A detailed illustration of the theoretical background and calculation procedures of the reliability analysis approach adopted in EN 1990 can be found by Afshan et al. [26].

The key statistical parameters for the analysis of the existing design methods and the CSM are summarized in Table 3, including the total number of tests and FE simulations n, the design (ultimate limit state) fractile factor $k_{d,n}$ which is related to the number of tests and FE

simulations in the dataset, the mean value of the correction factor b, the coefficient of variation of the tests and FE simulations relative to the resistance model V_δ, the combined coefficient of variation incorporating both model and basic variable uncertainties V_r and the required partial safety factor γ_{M0}. Note that the parameter b is taken as the average of the ratios of the test and FE resistances to the theoretical (predicted) values, as given in Eq. (28), in which n is the total number of the tests and FE simulations, r_e is the experimental or FE resistance and r_t is the theoretical (predicted) resistance. This definition (Eq. (28)) does not bias the value of b towards the test or FE results with higher failure resistance, which is unlike the least squares method adopted in Annex D of EN 1990 [25]. The values of material and geometric variables adopted in the analysis were taken as those recommended by Byfield and Nethercot [27], namely the material over-strength, i.e. the mean-to-nominal yield strength ratio (1.16), and the coefficients of variation of yield strength (0.05) and geometric properties (0.03). Similar values were adopted in a recent study by Tankova et al. [28].

$$b = \frac{1}{n} \sum_{i=1}^{n} \frac{r_{e,i}}{r_{t,i}} \qquad (28)$$

According to the results presented in Table 3, the CSM partial safety factors γ_{M0} of 1.09, 1.16 and 1.10, for hot-rolled steel I-sections under major axis bending plus compression, minor axis bending plus compression and biaxial bending plus compression, respectively, are all lower than the values obtained for EC3, but larger than the values obtained for the AISC Specification and also larger than the target value of 1.0. The more stocky hot-rolled steel I-sections with lower ratios of axial load to minor axis bending develop significant strain hardening, resulting in a high COV value (0.13) and hence a high required partial safety factor (1.16) based on the total test and FE population. However, the partial safety factor can be reduced by performing

the reliability analysis on two sub-sets [25] of the data for I-sections under minor axis bending plus compression based on the applied combination of loading, achieving reduced partial safety factors of 1.07 for $\theta > 10°$ and 1.00 for $\theta \leq 10°$. The average value of the ratios of the test and FE resistances to the CSM predictions (i.e. the parameter b) is significantly lower than those values obtained for EC3 and the AISC Specification, revealing improved accuracy in the CSM resistance predictions. The CSM generally provides more consistent predictions (i.e. lower V_δ values) and requires lower partial safety factors γ_{M0} than the corresponding values of EC3, and may therefore be considered to be a safe and economical design method.

5. Conclusions

A comprehensive parametric study, using the finite element models validated in the companion paper [16], on hot-rolled steel I-sections subjected to combined axial load and bending moment has been presented. A total of 1600 numerical results, covering a range of steel grades, cross-section slenderness values, cross-section aspect ratios and combinations of compression and bending moment, have been generated. Based on the experimental results from the companion paper [16] and the numerical results generated herein, the accuracy of the current design methods set out in EC3 [1] and AISC Specification [2] have been evaluated. The provisions of these specifications were found to be unduly conservative in predicting the cross-section resistance of hot-rolled steel I-sections under combined compression and bending moment due primarily to the conservative resistance predictions of pure compression and bending in isolation, which serve as the end points of the interaction curves. The continuous strength method (CSM) has been found previously to provide more accurate and consistent resistance predictions for hot-rolled steel cross-sections in compression and bending than the codified design methods, and the CSM has been extended herein to cover the design of hot-rolled steel I-sections under combined compression and bending. Comparisons with the experimental and

numerical data revealed that the proposed CSM approach generally results in a higher degree of accuracy and consistency in the resistance predictions than the existing design provisions, especially for very stocky cross-sections and for Class 3 cross-sections. The reliability of the CSM was also confirmed following statistical analyses performed in accordance with EN 1990.

Acknowledgements

Notation

The following symbols are used in this paper:

A = cross-section area;

A_f = flange area;

A_w = web area;

a = ratio of web area to gross cross-section area, as defined in EN 1993-1-1;

$a_{csm.f}$ = parameter related to the ratio of flange area to gross cross-section area;

$a_{csm.w}$ = parameter related to the ratio of web area to gross cross-section area;

B = width of section;

b = mean value of correction factor;

C_1 and C_2 = coefficients corresponding to the quad-linear material model;

c = flat width of the most slender constituent plate element in cross-section under compression;

E = Young's modulus;

E_{sh} = strain hardening modulus;

$f_{C_1\varepsilon_u}$ = stress corresponding to strain at $C_1\varepsilon_u$;

f_{csm} = CSM limiting stress corresponding to CSM strain;

f_u = ultimate tensile stress;

f_y = yield stress;

H = height of section;

$k_{d,n}$ = design fractile factor for n data points

M_c = nominal cross-sectional bending resistance according to AISC 360-16;

M_{csm} = CSM bending resistance;

M_{Ed} = applied design bending moment;

M_{el} = elastic moment capacity;

M_N = reduced plastic moment resistance;

M_{pl} = plastic moment capacity;

$M_{R,csm}$ = reduced CSM bending resistance;

N_c = nominal cross-sectional compression resistance according to AISC 360-16;

N_{csm} = CSM compression resistance;

N_{Ed} = applied design axial load;

N_u = ultimate axial load;

$N_{u,AISC}$ = predicted ultimate axial load according to AISC 360-16;

$N_{u,csm}$ = predicted ultimate axial load according to CSM;

$N_{u,EC3}$ = predicted ultimate axial load according to EC3;

$N_{u,pred}$ = predicted ultimate axial load;

$N_y = A f_y$ is the axial yield load;

$n = N_{Ed}/N_y$ is the ratio of design axial load to yield load and total number of tests and FE simulations;

$n_{csm} = N_{Ed}/N_{csm}$ is the ratio of design axial load to CSM compression resistance;

r_e = experimental resistance;

r_i = web-flange internal corner radius;

r_t = theoretical (predicted) resistance;

t_w = web thickness;

V_r = combined coefficient of variation;

V_δ = coefficient of variation of test results relative to resistance model;

W_{el} = elastic section modulus;

W_{pl} = plastic section modulus;

α = EN 1993-1-1 interaction power parameter and CSM coefficient in bending equation;

β = EN 1993-1-1 interaction power parameter and CSM coefficient in bending equation;

α_{csm} and β_{csm} = CSM interaction power parameters;

γ_{M0} = partial factor for cross-section resistance;

ε_{csm} = CSM maximum strain that a cross-section can sustain;

ε_{sh} = strain hardening strain where strain hardening initiates;

ε_u = strain at ultimate tensile stress;

$\varepsilon_y = f_y/E$ is the yield strain;

θ = angle parameter;

$\overline{\lambda}_p = \sqrt{f_y/\sigma_{cr}}$ is the cross-section slenderness;

σ_{cr} = elastic buckling stress of cross-section under applied loading conditions;

Suffix 'Rd' denotes design resistance;

Suffixes 'y' and 'z' denote bending about major and minor axis, respectively, and

Suffixes 'test' and 'FE' denote results obtained from experiments or FE models, respectively.

References:

[1] EN 1993-1-1. Eurocode 3: Design of steel structures – Part 1-1: General rules and rules for buildings. Brussels: European Committee for Standardization (CEN); 2005.

[2] ANSI/AISC 360-16. Specification for structural steel buildings. Chicago, Illinois: American Institute of Steel Construction (AISC); 2016.

[3] Bradford MA. Inelastic local buckling of fabricated I-beams. J Constr Steel Res 1987;7(5):317-34.

[4] Beg D, Hladnik L. Slenderness limit of class 3 I cross-sections made of high strength steel. J Constr Steel Res 1996;38(3):201-17.

[5] Dawe JL, Kulak GL. Local buckling behaviour of beam-columns. J Constr Steel Res 1986;112(11):2447-61.

[6] Kettler M. Elastic-plastic cross-sectional resistance of semi-compact H-and hollow sections. PhD thesis, Faculty of Civil Engineering, Graz University of Technology, Graz, Austria; 2008.

[7] Salem AH, El Aghoury M, El Dib FF, Hanna MT. Post local buckling strength of bi-axially loaded slender I-section columns. Thin-walled Struct 2005;43(7):1003-19.

[8] Hasham AS, Rasmussen KJR. Interaction curves for locally buckled I-section beam-columns. J Constr Steel Res 2002;58(2):213-41.

[9] Hasham AS, Rasmussen KJR. Section capacity of thin-walled I-section beam-columns. J Struct Eng 1998;124(4):351-59.

[10] Afshan S, Gardner L. The continuous strength method for structural stainless steel design. Thin-walled Struct 2013;68:42-49.

[11] Liew A, Gardner L. Ultimate capacity of structural steel cross-sections under compression, bending and combined loading. Structures 2015;1:2-11.

[12] Su MN, Young B, Gardner L. The continuous strength method for the design of aluminium alloy structural elements. Eng Struct 2016;122:338-48.

[13] Yun X, Gardner L. Stress-strain curves for hot-rolled steels. J Constr Steel Res 2017;133:36-46.

[14] Yun X, Gardner L, Boissonnade N. The continuous strength method for the design of hot-rolled steel cross-sections. Eng Struct 2018;157:179-191.

[15] Gardner L,Yun X, Macorini L, Kucukler M. Hot-rolled steel and steel-concrete composite design incorporating strain hardening. Structures 2017;9:21-28.

[16] Yun X, Gardner L, Boissonnade N. Ultimate capacity of I-sections under combined loading – Part 1: Experiments and FE model validation. J Constr Steel Res 2017; (Submitted).

[17] Seif M, Schafer BW. Local buckling of structural steel shapes. J Constr Steel Res 2010;66(10):1232-47.

[18] Taras A, Greiner R, Unterweger H. Proposal for amended rules for member bucking and semi-compact cross-section design. Technical Report, Consolidated version of documents of the same title submitted to the SC3 evolution group 1993-1-1, Paris; 2013.

[19] AISC Design Guide 27: Structural Stainless Steel. American Institute of Steel Construction; 2013.

[20] Design Manual for Structural Stainless Steel, 4th edition. The Steel Construction Institute (SCI), U.K.; 2017.

[21] Schafer BW, Ádány S. Buckling analysis of cold-formed steel members using CUFSM: conventional and constrained finite strip methods. Proceedings of the 18th International Specialty Conference on Cold-formed Steel Structures; Orlando, Florida, U.S.; 39-54; 2006.

[22] EN 1993-1-5. Eurocode 3: Design of steel structures – Part 1-5: Plated structural elements. Brussels: European Committee for Standardization (CEN); 2006.

[23] Zhao O, Rossi B, Gardner L, Young B. Behaviour of structural stainless steel cross-sections under combined loading – Part II: Numerical modelling and design approach. Eng Struct 2015;89:247-59.

[24] Arrayago I, Real E. Experimental study on ferritic stainless steel RHS and SHS cross-sectional resistance under combined loading. Struct 2015;4:69-79.

[25] EN 1990. Eurocode: Basis of structural design. Brussels: European Committee for Standardization (CEN); 2002.

[26] Afshan S, Francis P, Baddoo NR, Gardner L. Reliability analysis of structural stainless steel design provisions. J Constr Steel Res 2015;114:293-304.

[27] Byfield MP, Nethercot DA. Material and geometric properties of structural steel for use in design. Struct Eng 1997;75(21):393-67.

[28] Tankova, T., da Silva, L. S., Marques, L., Rebelo, C. and Taras, A. (2014). Towards a standardized procedure for the safety assessment of stability design rules. Journal of Constructional Steel Research. 103, 290-302.

Tables:

Table 1. Comparison of combined loading test and FE results with EC3, AISC and CSM capacity predictions

(a) Major axis bending plus compression			
No. of tests: 2	$N_{u,test/FE}/N_{u,EC3}$	$N_{u,test/FE}/N_{u,AISC}$	$N_{u,test/FE}/N_{u,csm}$
No. of FE simulations: 300			
Mean	1.07	1.09	1.05
COV	0.11	0.09	0.08
(b) Minor axis bending plus compression			
No. of tests: 2	$N_{u,test/FE}/N_{u,EC3}$	$N_{u,test/FE}/N_{u,AISC}$	$N_{u,test/FE}/N_{u,csm}$
No. of FE simulations: 300			
Mean	1.45	1.31	1.13
COV	0.31	0.11	0.13
(c) Biaxial bending plus compression			
No. of tests: 8	$N_{u,test/FE}/N_{u,EC3}$	$N_{u,test/FE}/N_{u,AISC}$	$N_{u,test/FE}/N_{u,csm}$
No. of FE simulations: 900			
Mean	1.46	1.41	1.12
COV	0.32	0.09	0.11

Table 2. Comparison of combined loading test results only with EC3, AISC and CSM capacity predictions

(a) Major axis bending plus compression			
No of tests: 2	$N_{u,test}/N_{u,EC3}$	$N_{u,test}/N_{u,AISC}$	$N_{u,test}/N_{u,csm}$
Mean	1.34	1.36	1.31
COV	0.04	0.04	0.01
(b) Minor axis bending plus compression			
No of tests: 2	$N_{u,test}/N_{u,EC3}$	$N_{u,test}/N_{u,AISC}$	$N_{u,test}/N_{u,csm}$
Mean	1.03	1.33	1.01
COV	0.04	0.04	0.05
(b) Biaxial bending plus compression			
No of tests: 8	$N_{u,test}/N_{u,EC3}$	$N_{u,test}/N_{u,AISC}$	$N_{u,test}/N_{u,csm}$
Mean	1.08	1.52	1.05
COV	0.03	0.03	0.03

Table 3. Summary of statistical parameters for the reliability analysis

Statistical parameters	Major axis bending plus compression			Minor axis bending plus compression			Biaxial bending plus compression		
	EC3	AISC	CSM	EC3	AISC	CSM	EC3	AISC	CSM
No. of FE (tests)	300(2)	300(2)	300(2)	300(2)	300(2)	300(2)	900(8)	900(8)	900(8)
$k_{d,n}$	3.123	3.123	3.123	3.123	3.123	3.123	3.040	3.040	3.040
b	1.069	1.086	1.054	1.453	1.305	1.128	1.463	1.408	1.119
V_δ	0.104	0.082	0.074	0.317	0.106	0.123	0.324	0.085	0.100
V_r	0.120	0.100	0.094	0.322	0.121	0.136	0.329	0.103	0.116
γ_{M0}	1.17	1.08	1.09	1.62	0.96	1.16	1.65	0.84	1.10

Figures:
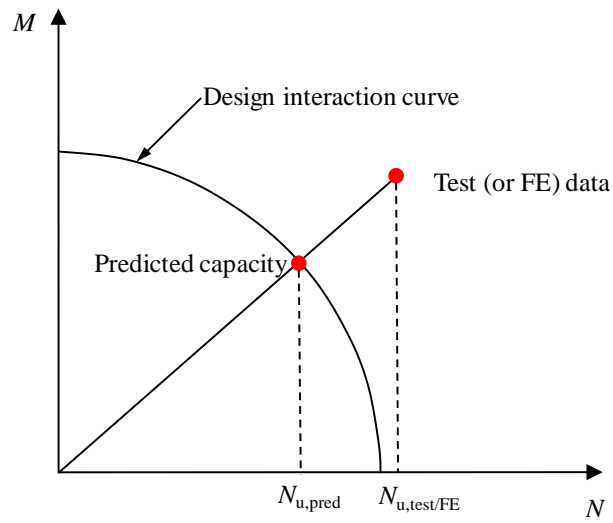
Fig. 1. Graphic definition of $N_{u,test/FE}$ and $N_{u,pred}$ for the assessment of design provisions
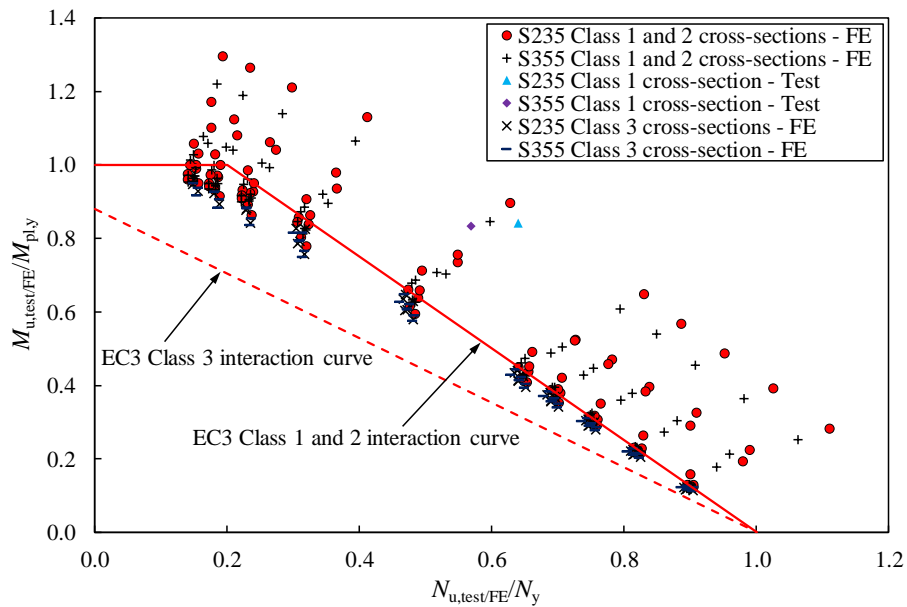
Fig. 2. Comparison of normalised test and FE results with EC3 interaction curves for hot-rolled steel I-sections in major axis bending plus compression
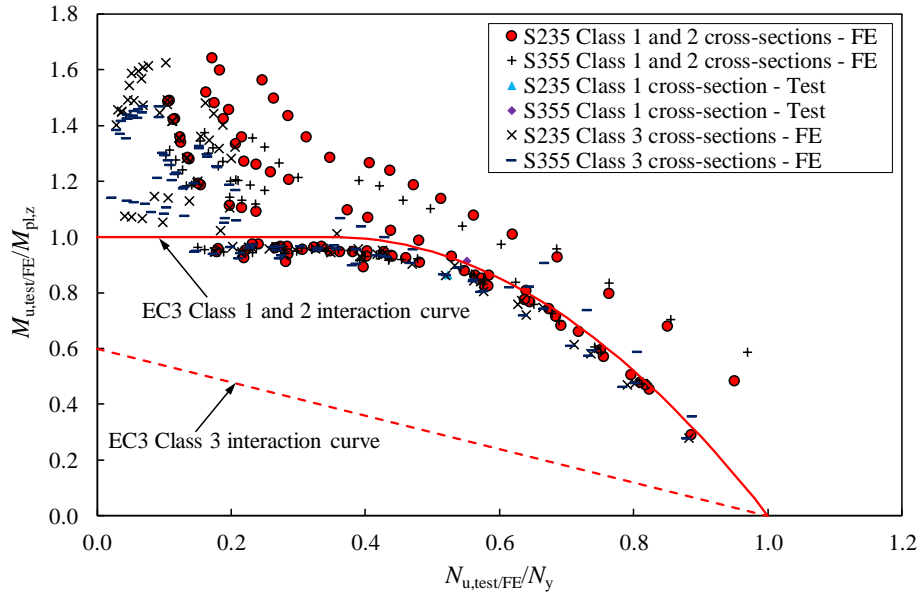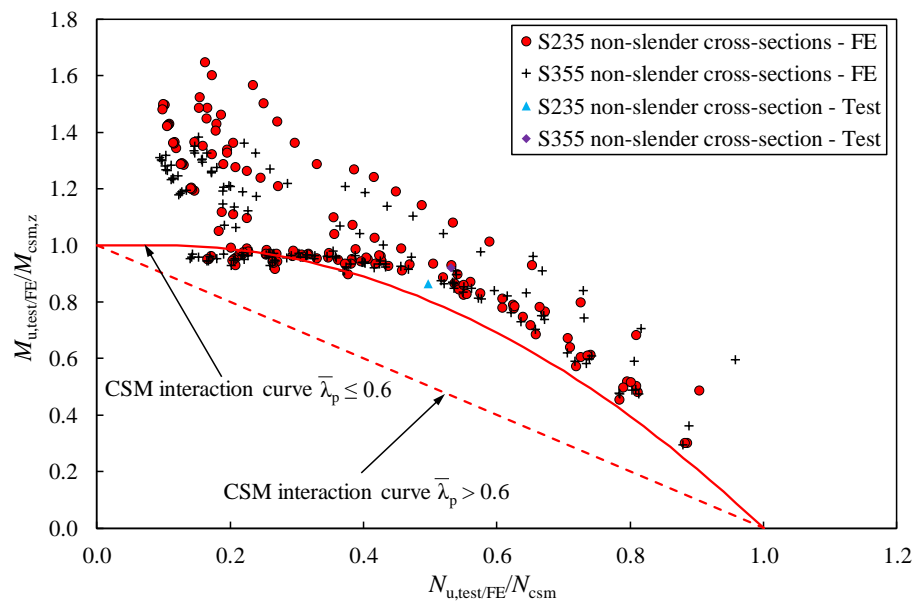
Fig. 3. Comparison of normalised test and FE results with EC3 interaction curves for hot-rolled steel I-sections in minor axis bending plus compression
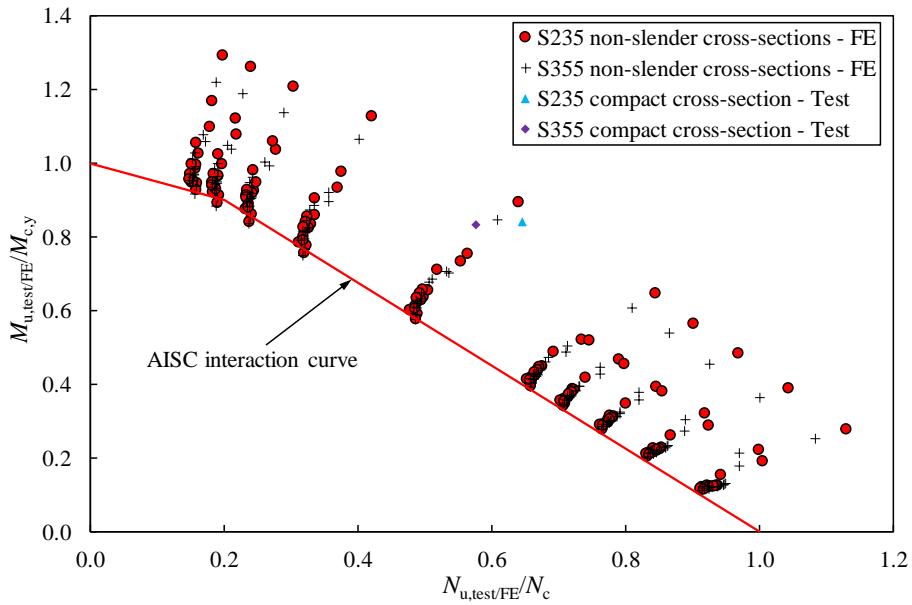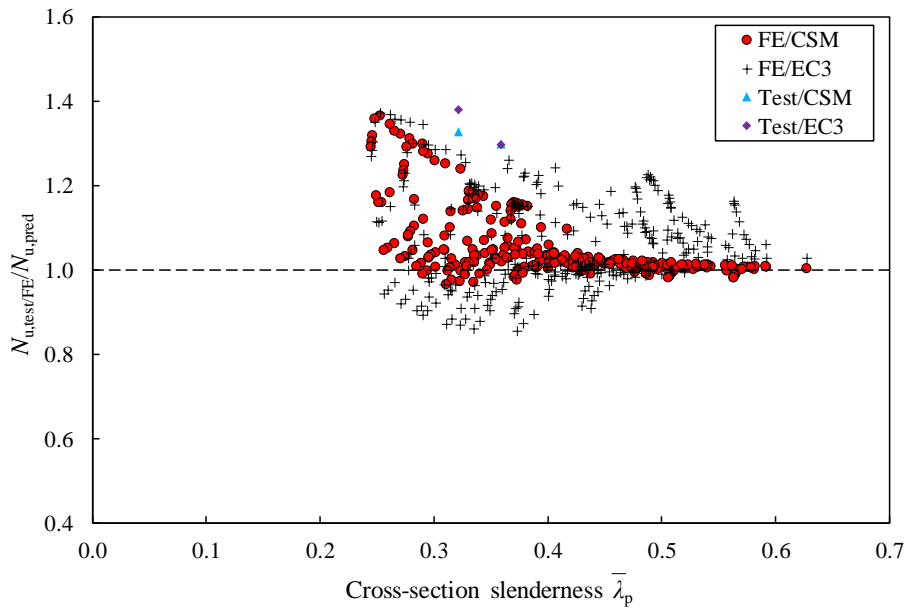

Fig. 4. Comparison of normalised test and FE results with AISC interaction curve for hot-rolled steel I-sections in major axis bending plus compression
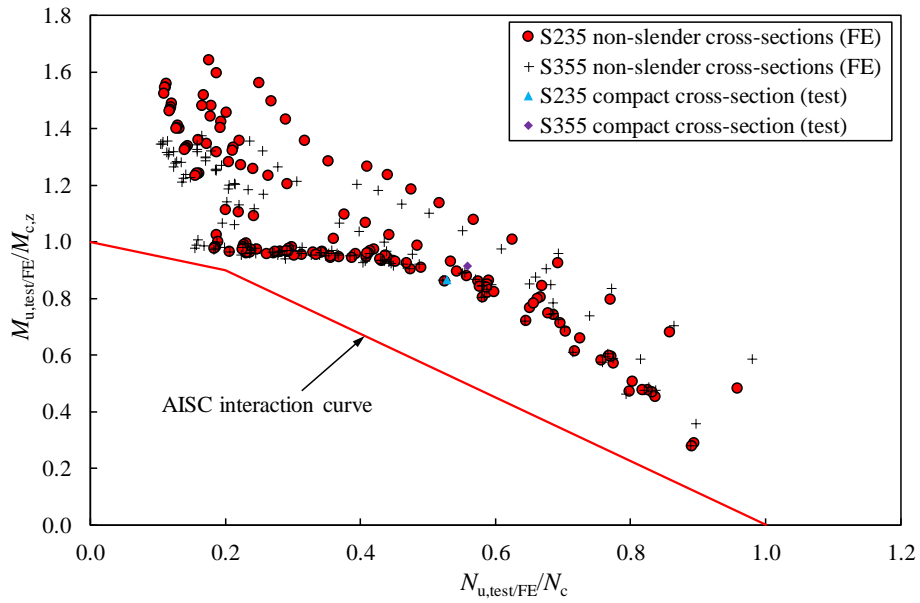
Fig. 5. Comparison of normalised test and FE results with AISC interaction curve for hot-rolled steel I-sections in minor axis bending plus compression
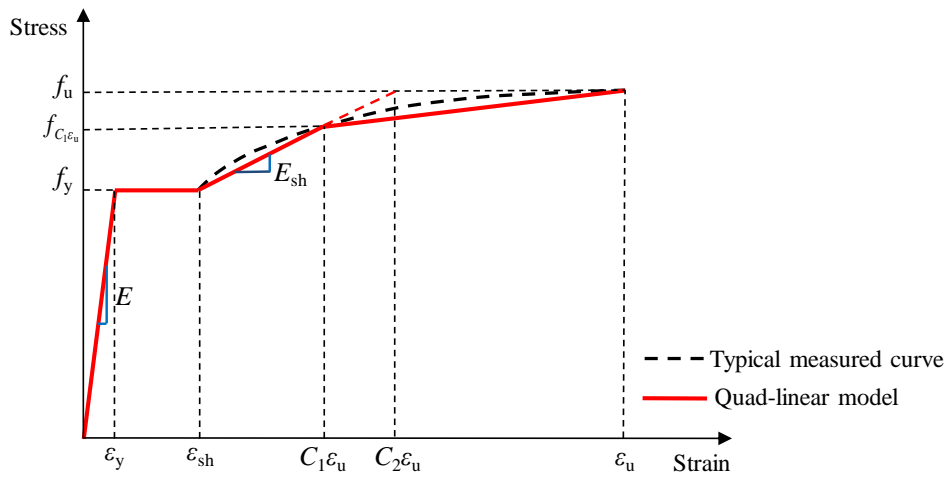
Fig. 6. Typical measured stress-strain curve and quad-linear material model for hot-rolled steels
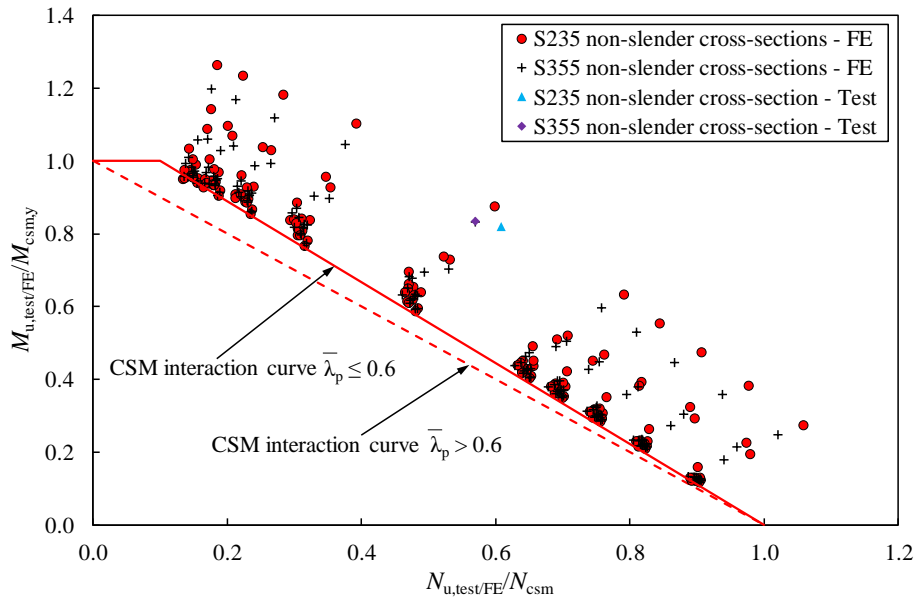
Fig. 7. Comparison of normalised test and FE results with CSM interaction curves for hot-rolled steel I-sections in major axis bending plus compression

Fig. 8. Comparison of normalised test and FE results with CSM interaction curves for hot-rolled steel I-sections in minor axis bending plus compression

Fig. 9. Comparison of test and FE results with predicted strengths from EC3 and CSM for hot-rolled steel I-sections in major axis bending plus compression (data arranged with respect to the cross-section slenderness $\bar{\lambda}_p$)
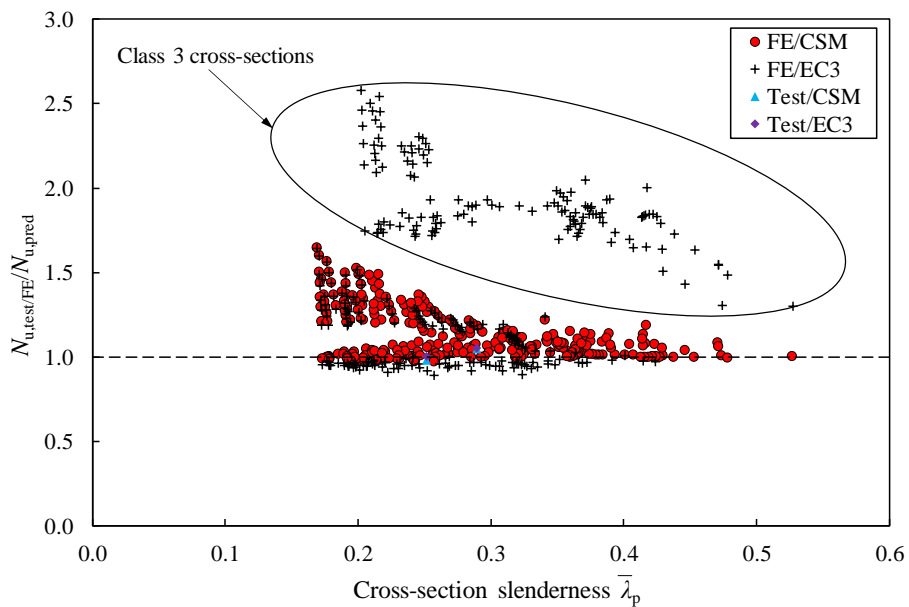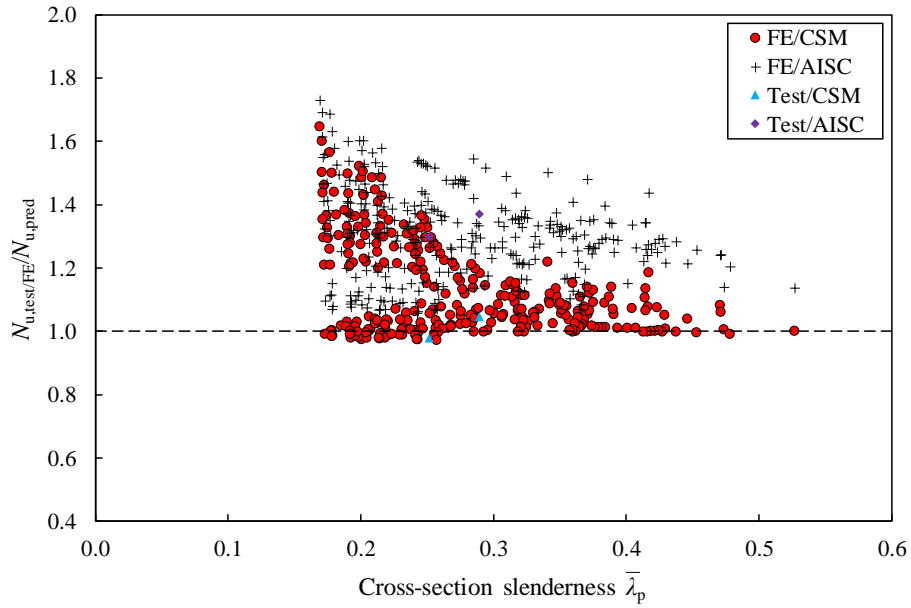

Fig. 10. Comparison of test and FE results with predicted strengths from EC3 and CSM for hot-rolled steel I-sections in minor axis bending plus compression (data arranged with respect to the cross-section slenderness $\bar{\lambda}_p$)
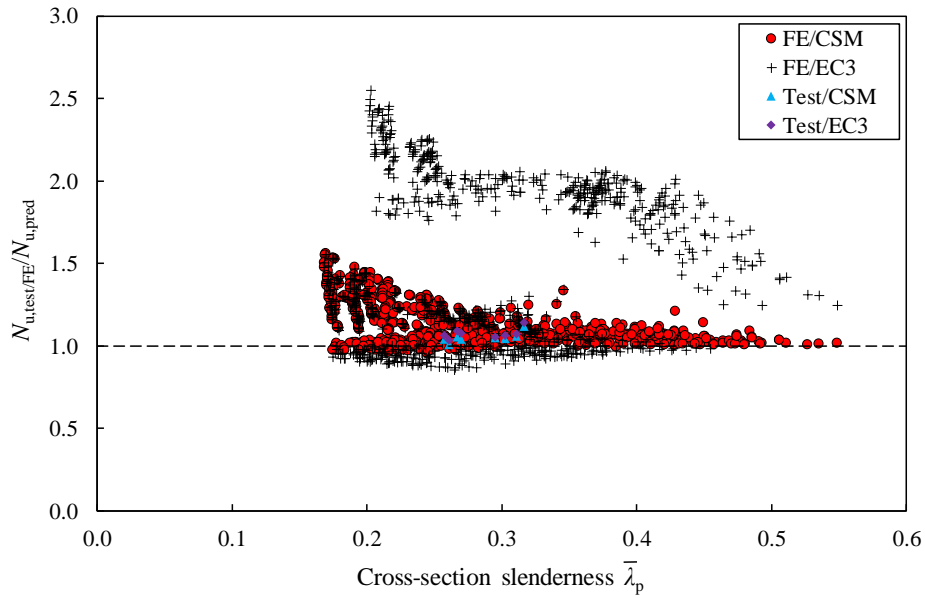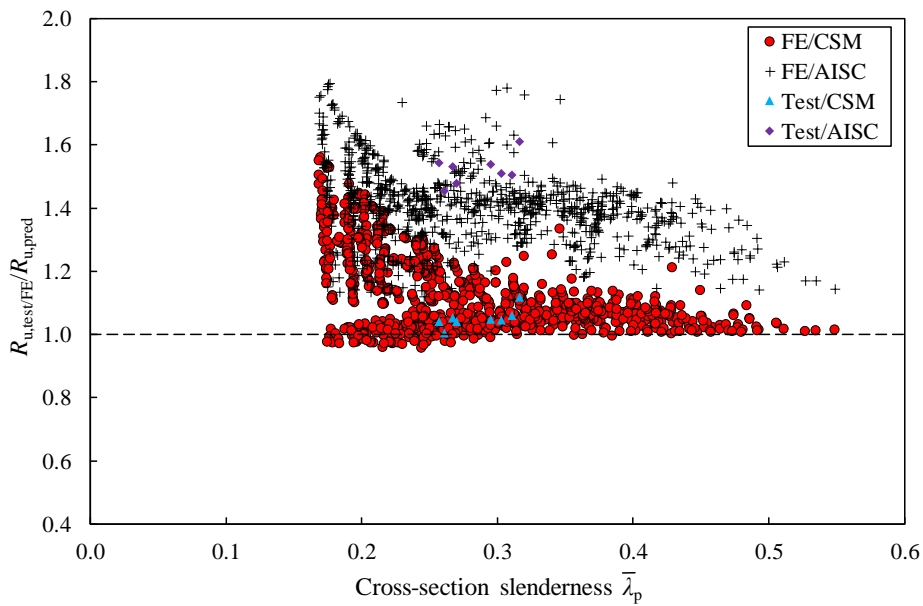
Fig. 11. Comparison of test and FE results with predicted strengths from EC3 and CSM for hot-rolled steel I-sections in biaxial bending plus compression
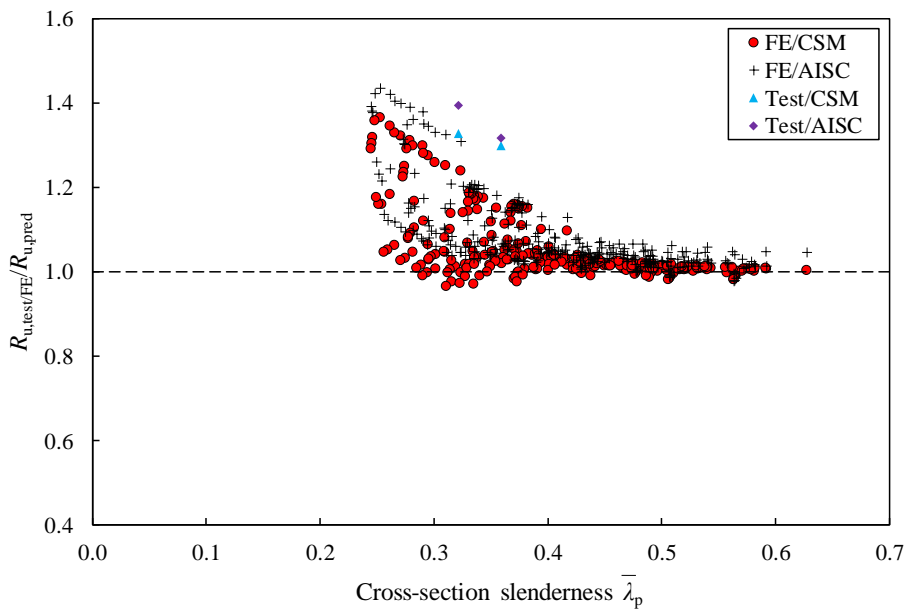
Fig. 12. Comparison of test and FE results with predicted strengths from AISC Specification and CSM for hot-rolled steel I-sections in major axis bending plus compression (data arranged with respect to the cross-section slenderness $\bar{\lambda}_p$)

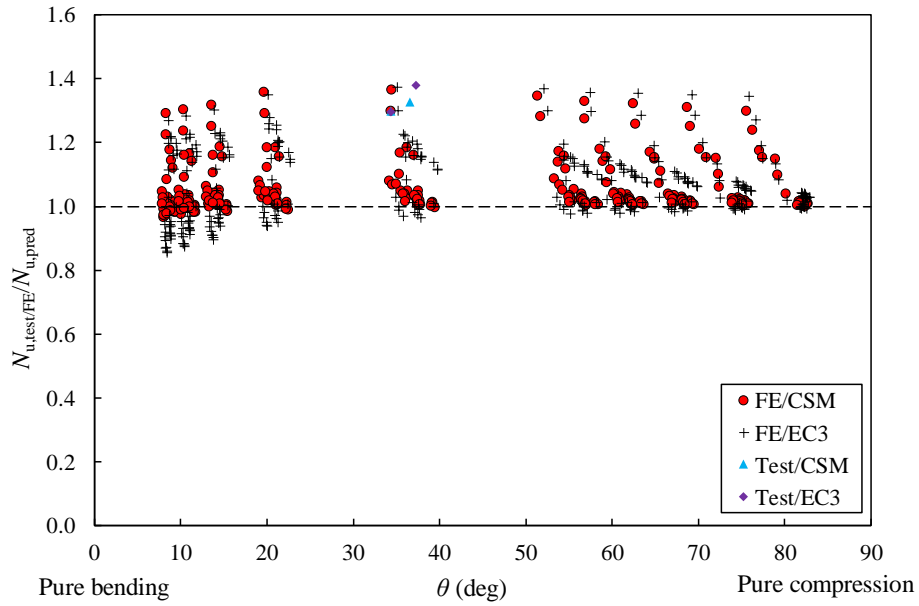**Fig. 13.** Comparison of test and FE results with predicted strengths from AISC Specification and CSM for hot-rolled steel I-sections in minor axis bending plus compression (data arranged with respect to the cross-section slenderness $\bar{\lambda}_p$)

Fig. 14. Comparison of test and FE results with predicted strengths from AISC Specification and CSM for hot-rolled steel I-sections in biaxial bending plus compression

Fig. 15. Comparison of test and FE results with predicted strengths from EC3 and CSM for hot-rolled steel I-sections in major axis bending plus compression (data arranged with respect to the angle parameter θ)
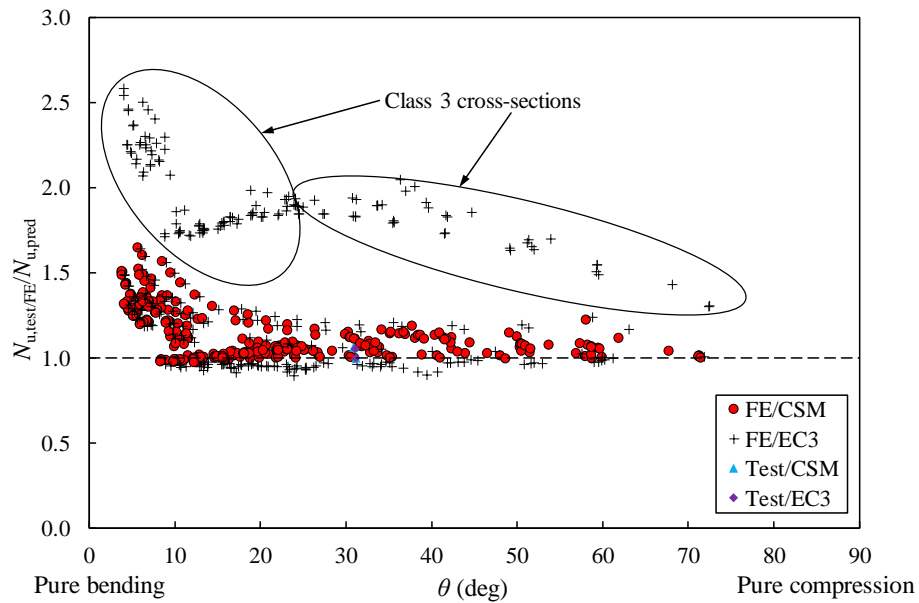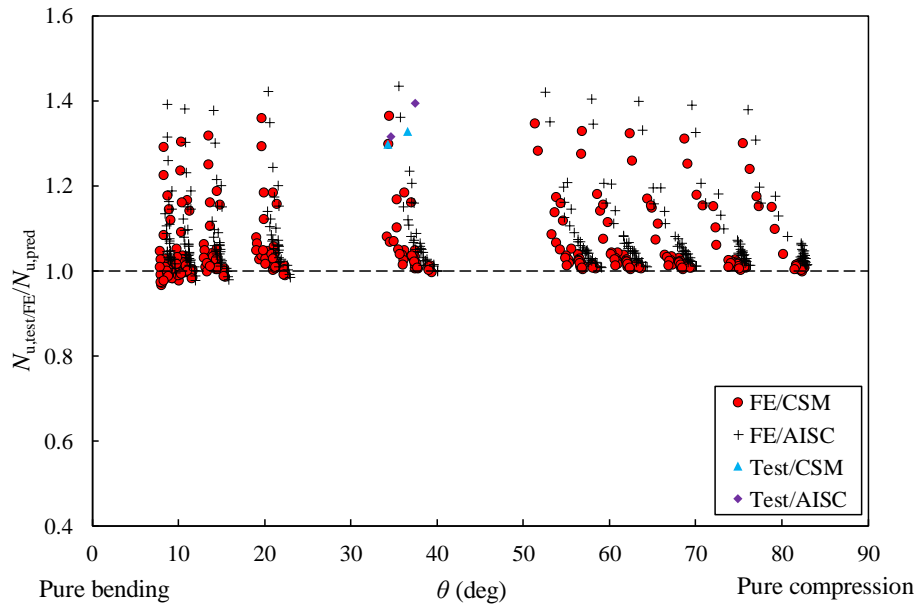

Fig. 16. Comparison of test and FE results with predicted strengths from EC3 and CSM for hot-rolled steel I-sections in minor axis bending plus compression (data arranged with respect to the angle parameter θ)

Fig. 17. Comparison of test and FE results with predicted strengths from AISC Specification and CSM for hot-rolled steel I-sections in major axis bending plus compression (data arranged with respect to the angle parameter θ)
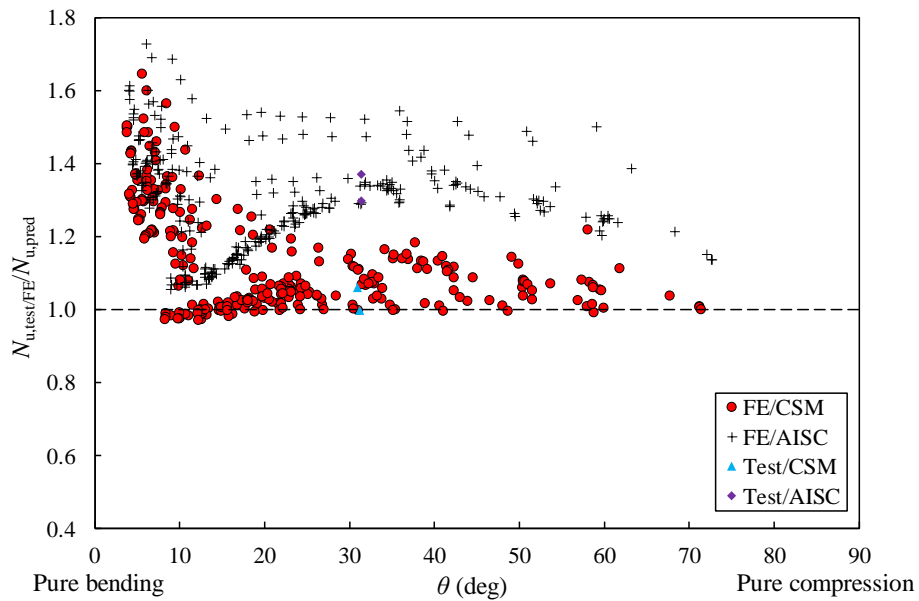

Fig. 18. Comparison of test and FE results with predicted strengths from AISC Specification and CSM for hot-rolled steel I-sections in minor axis bending plus compression (data arranged with respect to the angle parameter θ)
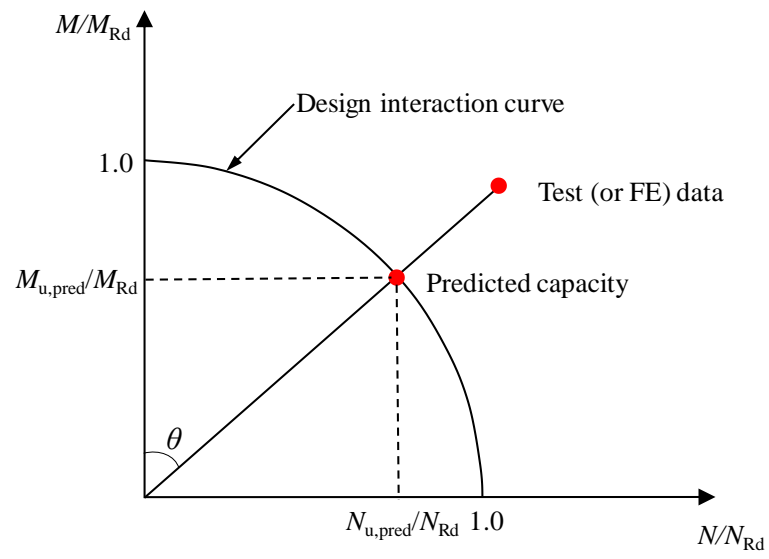
Fig. 19. Definition of θ on moment–axial load interaction curve